1 **Drone-derived canopy height predicts biomass across non-forest**
2 **ecosystems globally**

3

4 **<u>Contributors</u>**

5 Cunliffe, A.M.(1), Anderson, K.(2), Boschetti, F.(1), Brazier, R.E.(1), Graham, H.A.(1),
6 Myers-Smith, I.H.(3), Astor, T.(4), Boer, M.M.(5), Calvo, L.(6), Clark, P.E.(7), Cramer,
7 M.D.(8), Encinas-Lara, M.S.(9), Escarzaga, S.M.(10), Fernández-Guisuraga, J.M.(6), Fisher,
8 A.G.(11), Gdulová, K.(12), Gillespie, B.M.(13), Griebel, A.(5), Hanan, N.P.(14), Hanggito,
9 M.S.(10), Haselberger, S.(15), Havrilla, C.A.(16), Heilman, P.(17), Ji, W.(14), Karl, J.W.(18),
10 Kirchhoff, M.(19), Kraushaar, S.(15), Lyons, M.B.(20), Marzolff, I.(21), Mauritz, M.E.(10),
11 McIntire, C.D.(22), Metzen, D.(5), Méndez-Barroso, L.A.(9), Power, S.C.(8), Prošek, J.(12),
12 Sanz-Ablanedo, E.(23), Sauer, K.J.(24), Schulze-Brüninghoff, D.(4), Šímová, P.(12), Sitch,
13 S.(1), Smit, J.L.(25), Steele, C.M.(14), Suárez-Seoane, S.(26), Vargas, S.A.(10), Villarreal,
14 M.L.(27), Visser, F.(28), Wachendorf, M.(4), Wirnsberger, H.(15), Wojcikiewicz, R.(14)

Affiliations

15

16   1: Department of Geography, College of Life and Environmental Sciences, University of

17   Exeter, Exeter, UK; 2: Environment and Sustainability Institute, University of Exeter, Penryn,

18   UK; 3: School of GeoSciences, University of Edinburgh, UK; 4: Grassland Science and

19   Renewable Plant Resources, Organic Agricultural Sciences, Universität Kassel, D-37213

20   Witzenhausen, Germany; 5: Hawkesbury Institute for the Environment, Western Sydney

21   University, Penrith, Australia; 6: Biodiversity and Environmental Management Department,

22   Faculty of Biological and Environmental Sciences, University of León, León, Spain; 7:

23   Northwest Watershed Research Center, USDA Agricultural Research Service, Boise, Idaho,

24   USA; 8: Department of Biological Sciences, University of Cape Town, Cape Town, South

25   Africa; 9: Department of Environmental and Water Sciences, Instituto Tecnológico de

26   Sonora, Ciudad Obregón, Sonora, Mexico; 10: University of Texas at El Paso, El Paso,

27   Texas, USA; 11: Joint Remote Sensing Research Program, School of Earth and

28   Environmental Sciences, University of Queensland, Brisbane, QLD, 4072, Australia; 12:

29   Faculty of Environmental Sciences, Czech University of Life Sciences Prague, Kamýcká

30   129, Praha - Suchdol, 165 00, Czechia; 13: Biology Department, San Diego State University,

31   San Diego, California, USA; 14: New Mexico State University, Las Cruces, New Mexico,

32   USA; 15: Department of Geography and Regional Research, University of Vienna, Vienna,

33   Austria; 16: Northern Arizona University, Arizona, USA; 17: USDA-Agricultural Research

34   Service, Southwest Watershed Research Center, Tucson, AZ, USA; 18: University of Idaho,

35   Department of Forest, Rangeland, and Fire Sciences, Idaho, USA; 19: Department of

36   Physical Geography, Trier University, Germany; 20: School of Biological, Earth and

37   Environmental Sciences, University of New South Wales, Australia; 21: Department of

38   Physical Geography, Goethe University Frankfurt am Main, Germany; 22: Biology, University

39   of New Mexico, Albuquerque, New Mexico, USA; 23: Grupo de Investigación en Geomática

40   e Ingeniería Cartográfica (GEOINCA), University of León, Ponferrada, Spain; 24:

41   Department of Natural Resources, Sul Ross State University, Alpine, Texas, USA; 25:

42   Geomatics Division, School of Architecture, Planning and Geomatics, University of Cape

43   Town, Cape Town, South Africa; 26: Department of Organisms and Systems Biology

44   (Ecology Unit) and Research Unit of Biodiversity (UO-CSIC-PA), University of Oviedo,

45   Oviedo, Mieres, Spain; 27: U.S. Geological Survey, Western Geographic Science Center,

46   Moffett Field, CA 94035, USA; 28: School of Science and the Environment, University of

47   Worcester, Worcester, UK.

48   *correspondence to a.cunliffe@exeter.ac.uk

49 **Abstract**

50 Non-forest ecosystems, dominated by shrubs, grasses and herbaceous plants, provide

51 ecosystem services including carbon sequestration and forage for grazing, yet are highly

52 sensitive to climatic changes. Yet these ecosystems are poorly represented in remotely-

53 sensed biomass products and are undersampled by *in-situ* monitoring. Current global

54 change threats emphasise the need for new tools to capture biomass change in non-forest

55 ecosystems at appropriate scales. Here we assess whether canopy height inferred from

56 drone photogrammetry allows the estimation of aboveground biomass (AGB) across low-

57 stature plant species sampled through a global site network. We found mean canopy height

58 is strongly predictive of AGB across species, demonstrating standardised photogrammetric

59 approaches are generalisable across growth forms and environmental settings. Biomass

60 per-unit-of-height was similar *within,* but different *among,* plant functional types. We find

61 drone-based photogrammetry allows for monitoring of AGB across large spatial extents and

62 can advance understanding of understudied and vulnerable non-forested ecosystems across

63 the globe.

64

69 **Introduction**

70   Non-forest ecosystems, dominated by shrub and herbaceous plants, cover about 70% of the

71   Earth's land surface[1] and account for around 35% of all aboveground biomass (AGB)[2]. They

72   provide multiple ecosystem services, playing dominant roles in the long-term trends and

73   interannual variability of the global carbon cycle[3,4], and are highly significant for grazing and

74   agriculture[5]. Grassland, shrubland, Arctic tundra, savanna and proglacial montane

75   landscapes are often more sensitive and respond faster to changes in climate than forests[6],

76   but have received less systematic research attention[1,7,8]. Non-destructive measurements of

77   canopy height and biomass are fundamental requirements for plant science[9–11] to

78   understand the roles of these ecosystems in climate change mitigation, sustainable food

79   production and land management[12–14]. However, measuring biomass with *in situ*

80   measurements is labour intensive and thus prone to undersampling, particularly in

81   ecosystems that are spatially heterogeneous and/or temporally dynamic, putting on (and

82   losing) biomass rapidly[1,15–17]. Gaps in available data mean that biomass dynamics are not

83   being captured in many important ecosystems across the globe, hindering the calibration

84   and validation of vegetation models and products derived from satellite observations[7,14]. The

85   lack of accurate biomass data limits our ability to track changes and predict future responses

86   in globally relevant non-forest ecosystems.

87

88   Improving the accuracy of biomass data in non-forest biomes requires approaches that are:

89   (i) sensitive to small differences in AGB, (ii) sufficiently inexpensive to be adopted worldwide,

90   and allow (iii) spatially continuous sampling across (iv) representative areas at (v) temporal

91   frequencies appropriate for dynamic ecosystems[14,16]. The most accurate non-destructive

92   estimates of AGB are generally obtained from *in situ* measurements of attributes such as

93   plant cover, height and stem diameters, using allometric functions fitted to harvested

94   biomass observations. Canopy volume, the product of height and cover, is often the

95   strongest predictor of AGB for shrubs, herbs and other low-stature plants[15,18–22]. Remote-

96   sensing approaches have been widely used to extend the coverage of biomass predictions.

97   Biomass can be predicted from airborne LiDAR (Light Detection and Ranging) in shrublands

98   and savannas[23], but the footprints sampled by LiDAR can be insensitive to fine-scale

99   changes in plant structure and these data are expensive and unavailable in many areas.

100   Biomass estimates computed from spectral reflectance are often highly uncertain due to

101   asymptotic relationships between AGB and surface reflectance and variable soil albedo[6,22].

102   Globally-available biomass products from space-based sensors such as LiDAR, synthetic-

103   aperture radar or vegetation optical depth are either insensitive and/or poorly calibrated and

104   validated in low-biomass (<20 Mg ha^{-1}) ecosystems[1,7,8,14,24].

105

106   Photogrammetry using aerial images acquired with unmanned aerial systems (UAS, herein

107   'drones') could greatly improve quantification of AGB in non-forest ecosystems, both directly

108   at a local scale and indirectly by improving the calibration and validation of biomass products

109   obtained from coarser scale remotely-sensed observations. Advances in photogrammetry,

110   particularly structure-from-motion (SfM) with multi-view stereopsis[25], have made it possible

111   to capture 3D representations of plants, quantitatively describing their fine-scale structure

112   with an unprecedented level of detail[26,27]. SfM allows objective measurements of canopy

113   height at sub-decimetre spatial grain for a wide range of plant growth forms[18–20,27–31].

114   Lightweight and inexpensive drones enable vegetation sampling at temporal intervals

115   appropriate for highly dynamic ecosystems[16,32] and can be used for detailed surveys over

116   extents of 1-10 ha, covering more representative areas of heterogeneous ecosystems[15,27]

117   that allow spatially explicit comparison with other biomass estimates[1,14,32].

118

119   Fully realising the potential of drone photogrammetry in plant science requires reproducible

120   workflows, which minimise biases[30,33,34]. Over the past few years, thousands of hectares of

121   low-stature ecosystems have been surveyed with drones across the globe, yielding

122   information-rich datasets. However, drone-photogrammetry products are sensitive to the

123   ways in which data are (i) collected (e.g., ground sampling distance, image overlap, viewing

124   geometry, spatial control, illumination conditions)[27,30,34–38], (ii) processed (e.g., software, lens

125   model, specification of control accuracy, selection of processing quality, depth filtering)[27,36–

126   38], and (iii) analysed (e.g., canopy height metrics, spatial grain and interpolation, statistical

127   treatment)[20,27–29,31]. These sensitivities are more pronounced for subjects with complex

128   texture, such as vegetation, and hinder comparisons between products obtained from

129   different workflows. To maximise the value of these approaches, standardised and

130   reproducible protocols are needed, but few efforts currently exist to advance this aim.

131   Addressing critical knowledge gaps in plant science with drone photogrammetry requires

132   knowledge of the relationships between photogrammetrically derived canopy height and

133   AGB across the range of plants and ecosystems in which they will be applied, and

134   systematic understanding of the possible influences of environmental conditions (e.g. wind

135   speed and illumination)[19,27,30,35,39]. In this study, we apply a new, standardised approach for

136   airborne allometric inference of biomass for non-forested ecosystems globally using drone

137   photogrammetry. We asked the following research questions: (1) Does canopy height
138   derived from drone photogrammetry correspond with AGB at the species-level? (2) Does
139   photogrammetry-derived canopy height correspond with AGB at the PFT-level? (3) Are
140   relationships between reconstructed canopy height and biomass influenced by wind speed
141   and (4) and solar elevation?

142

143   Using rigorous, consistent protocols[33], we conducted a novel, globally coordinated
144   experiment to sample 36 sites, encompassing a diverse range of non-forest ecosystems,
145   including semi-arid and temperate grasslands and shrublands, Arctic tundra, savanna and
146   proglacial montane sites (Fig. 1B), spanning from 71° North to 37° South, across North
147   America, Europe, Australia and Africa (Fig. 1A). Our study includes photogrammetric
148   reconstructions from 38 different surveys (Supplementary Table 1), sampling 50 low-stature
149   plant species across six PFTs including ferns, forbs, graminoids, shrubs, succulents and
150   trees that cover phylogenetic diversity including non-flowering plants and the most species-
151   rich clades of flowering plants (including monocots and eudicots). To calibrate our allometric
152   models, we sampled 741 harvest plots, with AGB ranging from 9 g m^{-2} to 7,892 g m^{-2} and
153   mean (maximum) canopy heights ranging from 0 m to 1.9 m (0.01 m to 6.7 m). Our sample
154   achieved a more than twenty-fold improvement in the coverage of harvest plots, species and
155   sites compared to previous photogrammetry vegetation studies (Fig. 1C)[20,28,29]. We fitted
156   plant functional type (PFT) and species-specific models that predict AGB from fine-grained
157   canopy height as determined by SfM photogrammetry. Mean canopy height, sampled at fine
158   (centimetre) spatial grain, integrated canopy cover and height as well as foliage density. The
159   consideration of these multiple plant size attributes is key to robust prediction of biomass.

160
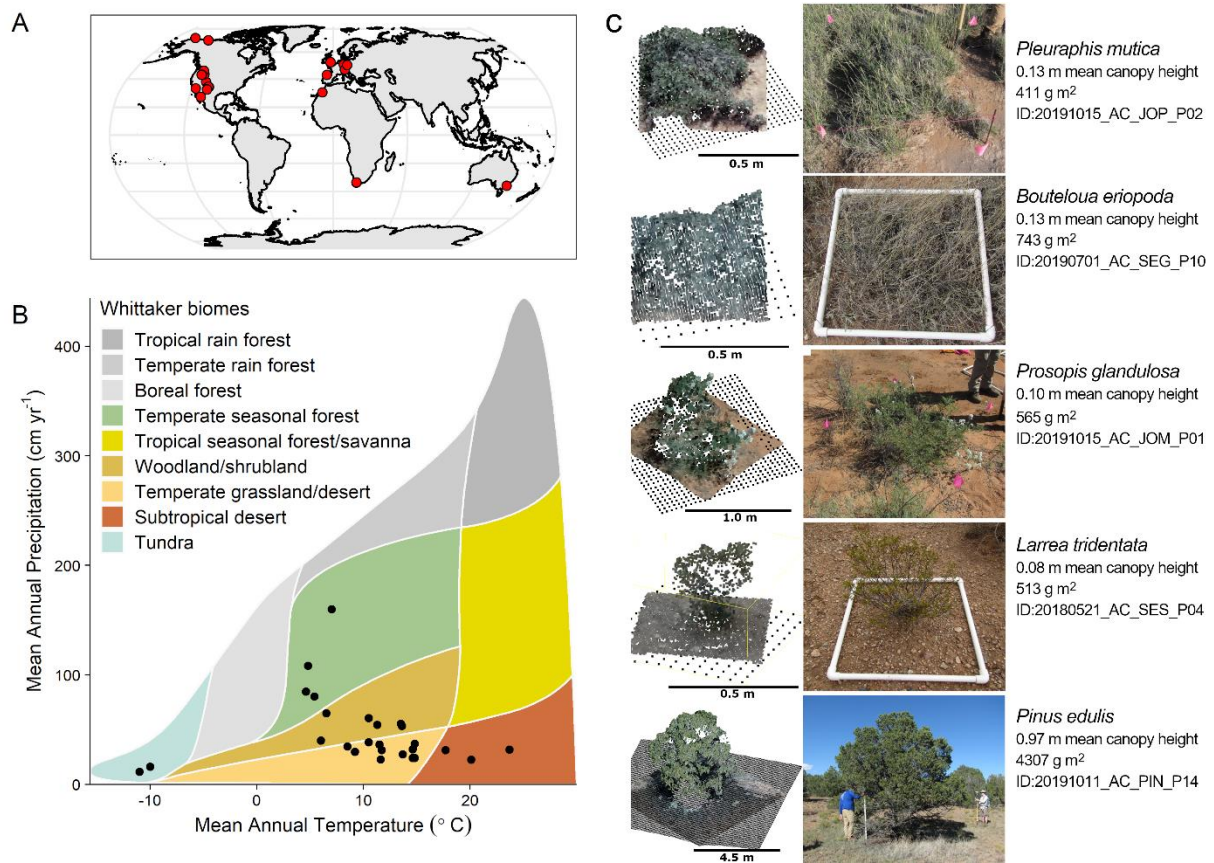
Fig. 1. Point clouds derived from drone surveys consistently provided structural reconstructions of plants across non-forested ecosystems. A depicts the geographic distribution of our sites, spanning four continents. **B** depicts the bioclimatic distribution of sites in terms of annual average precipitation and temperature. We sampled five biomes where low-stature vegetation is often dominant, representing every appropriate (non-forest) biome described by Whitaker[40]. **C** Reconstructed point clouds corresponded well with photographs of harvest plots. The grid of black points represents the underlying terrain model.

169   **Methods**

170   *Site and Species selection*

171   We focused our efforts on low-stature phenotypes in non-forest ecosystems, including

172   grasslands, shrublands with open and closed canopies, and woody savannas. Low-stature

173   ecosystems are understudied and tools for quantifying forest biomass are better represented

174   in the existing literature[1,7,8]. While photogrammetry can be used to characterise forest

175   canopies[30,31,35], we consider forest ecosystems better candidates for observation with active

176   remote sensing approaches such as synthetic-aperture radar[7], vegetation optical depth and

177   LiDAR[52]. We selected species that were regionally widespread, accessible and would inform

178   ongoing research efforts, but excluded extensively modified vegetation such as managed

179   hedges. Sampling was undertaken during seasonal peak canopy cover to minimise

180   differences arising from phenophase, although plant development and allometric

181   relationships may still vary especially in more water-limited ecosystems[41]. The data

182   collection protocol was comprehensively described by Cunliffe and Anderson[33]. Two study

183   sites ('SES' and 'SEG') were sampled on consecutive years, giving 38 surveys from 36 sites

184   (Supplementary Table 1).

185   *Aerial imaging surveys*

186   Harvest sites were surveyed using drones to acquire aerial red-green-blue images. For each

187   site, two sets of survey flights were undertaken, the first obtaining nadir imagery to attain a

188   spatial grain of ca. 5 mm per pixel at the canopy top, and the second obtaining oblique (ca.

189   20° from nadir) images from ca. 4 m higher. Survey altitudes varied depending on the

190   resolution and field-of-view of the sensors and the canopy height[30], but were typically 20 m

191   above the canopy. The different perspectives afforded by the nadir and slightly higher,

192   convergent surveys helps to improve the stability of the camera network[36,37,45,53–56]. Both

193   survey flights obtained 75% forward and side overlap, together capturing at least 30 images

194   for each part of the study area. The high image overlap facilitated tie point matching in the

195   vegetated scenes. Wind speeds were generally recorded using handheld anemometers

196   immediately prior to the survey[47]. Our sampling protocol[33] was optimised for smaller plants of

197   up to ca. 3 m in height. To support feature matching in texturally complex scenes containing

198   taller vegetation (e.g., mature *Juniperus monosperma* or *Pinus edulis*), higher survey

199   altitudes could be used to help minimise excessive parallax (i.e., excessive scene changes

200   between overlapping images).

201   A key requirement for photogrammetric surveys is the inclusion of adequate spatial

202   control[38,45]. Our photogrammetric reconstructions used thirteen ground markers, each

203   measuring ca. 20 cm x 20 cm, deployed across each site and geolocated to a typical

204   precision of ± 0.015 m horizontally and ± 0.03 m vertically. Further details on the sites and

205   survey equipment are provided in Supplementary Table 1. Images intended for

206   photogrammetric analysis should ideally not be geometrically corrected in-camera prior to

207   further distortion correction. Such in-camera processing is a problem for JPG-format image

208   files from cameras like the widely used DJI Phantom 4 Advanced/Pro FC6310 camera, and

209   so capturing RAW-format images can help avoid this error source[38,45]. We anticipate ongoing

210   improvements to camera geolocation and orientation information from drone systems will

211   continue to improve the accuracy and reliability of the camera parameter estimation,

212   particularly in densely vegetated and thus texturally complex settings (Supplementary Note

213   1)[34,38,45,57,58].

214   ***Vegetation harvests***

215   We used an area-based approach to enable sampling in ecosystems with continuous or

216   coalesced canopies, while also sampling individual plants where these were naturally

217   isolated from other plants[33,59]. We selected harvest plots to sample across the natural range

218   of canopy heights observed at each site, in order to estimate the allometric models more

219   efficiently as well as to test the form of the relationship between mean canopy height and

220   biomass[46]. Plots were chosen to try to ensure that ≥ 90% of the biomass and ≥ 90% of the

221   foliar volume within each plot were from the target species. We aimed for a minimum harvest

222   plot size of 0.5 m x 0.5 m to reduce the possible effects of co-registration errors[22]. The

223   corners of each plot were geolocated with high-precision GNSS before all standing biomass

224   was harvested to ground-level (or the moss level for *Salix richardsonii* and *Arctophila*

225   *fulva*)[22]. Biomass was then dried at ca. 50-80°C until reaching a constant weight over a 24-

226   hour period. For some of the largest taxa (*Adenostoma fasciculatum, Adenostoma*

227   *sparsifolium, Atriplex polycarpa, Ericameria nauseosa, Juniperus monosperma, Launaea*

228   *arborescens, Pinus edulis* and *Prosopis velutina*), freshly harvested biomass was weighed in

229   the field and representative sub-samples were then dried to determine moisture contents[59].

230   Plot areas were computed from corner coordinates, unless a quadrat was used during

231   harvesting in which case the area of the quadrat was used to minimise propagating errors

232   from GNSS-coordinates.

233   ***Image-based modelling***

234   Aerial images were processed using SfM photogrammetry, using established workflows and

235   following our previous studies[27,59]. Geotagged image data and ground-control marker

236   coordinates were imported into AgiSoft PhotoScan Professional v1.4.3 (now Metashape;

237   http://www.agisoft.com) and converted to UTM coordinate reference systems. Image

238   sharpness was measured using PhotoScan's image quality tool, all images had an image

239   sharpness score of ≥ 0.5[37]. Tie points were matched and cameras aligned using

240   PhotoScan's highest quality setting, a key point limit of 40,000, a tie point limit of 8,000, with

241   generic and reference pair preselection enabled, and adaptive camera model fitting disabled.

242   During camera self-calibration we enabled the following lens parameters: Focal length (f),

243   principal point (cx, cy), radial distortion (k1, k2), tangential distortion (p1, p2), aspect ratio

244   and skew coefficient (b1, b2). Most cameras had global shutters but rolling shutter

245   corrections were used when appropriate. Reference parameters were set to: camera

246   location accuracy = XY ± 20 m, Z ± 50 m; marker location accuracy = XY ± 0.02 m, Z ± 0.05

247   m; marker projection accuracy was set to 2 pixels; tie point accuracy was set to either the

248   mean root mean square reprojection error or one, whichever was greater. The result of

249   camera alignment was a sparse point cloud that was then filtered and points with

250   reprojection error above 0.45 pixels were excluded from further analysis. An operator

251   reviewed the sparse point clouds and estimated camera positions to verify their plausibility.

252   Any obviously erroneous tie points were removed manually. Geolocated markers were

253   placed by an operator on ten projected images for each of the 13 ground control points. Ten

254   of these markers were used to constrain the photogrammetric reconstructions spatially[60],

255   while the remaining three were used for independent evaluation of each reconstruction. The

256   three markers used for accuracy assessment were deselected before the interior and

257   exterior camera parameters were optimised. Any obviously implausible camera positions

258   were refined after marker placement and optimisation. All cameras were usually aligned and

259   used for multi-view stereopsis (dense point cloud generation), using the ultrahigh quality

260   setting with mild depth filtering to preserve finer details of the vegetation[27,29,30]. For further

261   discussion of some of the limitations of this approach, see Supplementary Note 1. Dense

262   point clouds were exported in the laz format, with point coordinate and RGB attributes.

263   *Digital terrain models*

264   An essential requirement for deriving canopy height models from photogrammetry-derived

265   point clouds is a digital terrain model, which must be sufficiently accurate and detailed with

266   respect to canopy heights and topographic complexity[31]. We used terrain models

267   interpolated with Delaunay triangulation between the GNSS-observations of the harvest plot

268   corners (Fig. 1C). In instances where plant canopies are discontinuous in space, suitable

269   terrain models may be extracted from the photogrammetric point cloud[20,27]. Other options

270   can include extracting terrain models from photogrammetric drone surveys during leaf-off

271   conditions (or post-harvest, if applicable), LiDAR surveys[61] or walkover surveys with GNSS

272   instruments.

Calculation of canopy heights

274   Point clouds were analysed with PDAL (v2.1.0)[62]. The point cloud representing each harvest

275   plot was subset using the GNSS-observed corner coordinates. In a few instances where plot

276   infrastructure (e.g., marker posts or flags) was visible in the point cloud (n=20 plots), these

277   points were manually assigned to a noise class and excluded from canopy height

278   calculations. Within each plot, the height-above-ground of each point was calculated relative

279   to the terrain model and any points with a negative height-above-ground were set to

280   zero[20,27]. Using a 0.01 m resolution grid, we calculated the maximum point height in each

281   grid cell. For cells containing no points, we interpolated heights using inverse distance

282   weighting considering an array of 7 × 7 cells using a power of one, and cells with no

283   neighbouring points in that area remained empty. Plot-level mean canopy height was then

284   extracted from this grid of local maxima elevations.

Statistical analysis

286   Statistical analyses were conducted in R v3.6.1[63]. Sun elevations during each survey were

287   computed with the Astral package[64]. We produced the climate space plot using the

288   plotbiomes R package[65] based on the biomes described by Whittaker[40]. We excluded 13

289   bryophyte plots from two rocky sites where we were unable to extract meaningful canopy

290   height observations (Supplementary Fig. 5) and 16 graminoid plots from one grassland site

291   ('WSP') that could not be reconstructed (Supplementary Fig. 6, Supplementary Note 1).

292   We used ordinary least squares regression to fit separate linear models predicting AGB

293   observations from mean canopy height for each PFT and for each species with four or more

294   observations. We considered ferns, forbs, graminoids, shrubs, trees and succulents as

295   PFTs, and constrained the y-intercept to zero in order to ensure zero canopy height

296   predicted zero biomass. Model performance was validated using leave-one-out cross-

297   validation (LOOCV) to compute the mean out-of-sample prediction error, which was divided

298   by the model slope to obtain relative errors for each model[31,66].

299   To test the influence of wind speed on allometric functions, we fitted a generalised linear

300   mixed model (GLMM) to predict total biomass as a function of canopy height and wind speed

301   as fixed-effects and PFT as a random-effect based on a gamma error distribution with an

302   identity link function, using the 'lme4' package (v1.1-23)[67] (Supplementary Table 3).

303   Succulents were excluded from this model because their inclusion prevented model

304   convergence, possibly because this PFT had a much steeper slope between height:biomass

305   (Table 1, Fig. 2) and/or because they may be less influenced by wind speed (Supplementary

306   Fig. 2A). To illustrate the effect of wind speed, we used the 'ggeffects' pacakge (v0.15)[68] to

307   simulate the relationship between height and biomass for three levels of wind speed using

308   the GLMM (Fig. 3A), and plotted the slope of biomass-height models (±83% confidence

309   interval[69]) against wind speed at the PFT- (Supplementary Fig. 2A) and species-levels

310   (Supplementary Fig. 3).

311   To test the influence of cloud cover on allometric functions, we fitted a linear mixed model

312   (LMM) to predict total biomass as a function of canopy height, with PFT as a random-effect

313   and cloud cover as fixed-effects, using the 'lmerTest' package (v3.1-2)[70] (Supplementary

314   Table 4). Cloud cover was coded as a binary factor, with relatively clear sky (n=620) and

315   cloudy conditions where the sun was obscured (n=80, sky codes ≥ 6 after[71], Supplementary

316   Table 6). To illustrate the effect of sun elevation, we simulated the modelled relationship

317   between height and biomass for the two levels of cloud cover using the LMM

318   (Supplementary Fig. 4).

319   To test the influence of sun elevation on allometric functions, we fitted a LMM to predict total

320   biomass as a function of canopy height and sun elevation as fixed-effects and PFT as a

321   random-effect, using the 'lmerTest' package (v3.1-2)[70] (Supplementary Table 5). We only

322   included observations (n=620) collected under relatively clear sky conditions (sky codes ≤ 5,

323   after[71]) when scene illumination was minimally modulated by clouds. To illustrate the effect

324   of sun elevation, we simulated the modelled relationship between height and biomass for

325   three levels of sun elevation using the LMM (Fig. 3B), and plotted the slope of biomass-

326   height models (±83% confidence interval[69]) against sun elevation at the PFT-

327   (Supplementary Fig. 3B) and species-level (Supplementary Fig. 5). There was insufficient

328   replication to allow convergence of more complex model structures including species nested

329   within PFT or site as random-effects. We evaluated diagnostics for all model visually using

330   the R package 'performance' (v0.4.6)[72].

Results

331

332   We found photogrammetrically measured mean canopy height was strongly predictive of

333   AGB at the species-level. Linear models with a zero-intercept provided good approximations

334   of the relationships between mean canopy height and AGB and are readily interpreted (Fig.

335   2, Supplementary Fig. 1)[22,31]. The slopes from these models are equivalent to AGB density

336   (g m^{-3}, calculated by dividing g m^{-2} by mean canopy height). Species-level densities ranged

337   between 375 g m^{-3} to 13,801 g m^{-3} (Supplementary Fig. 1, Supplementary Table 2). Mean

338   canopy height was an accurate predictor for individual species, especially when calibrated

339   for specific ecophenotypic and phenological conditions[15,31,41]. Model goodness-of-fit was

340   strong, with adjusted R^2 values ranging from 0.46 to 0.99 with a mean of 0.83

341   (Supplementary Fig. 1, Supplementary Table 2). Leave-one-out cross-validation indicated a

342   mean prediction error of 7.4% (Supplementary Table 2). The high goodness-of-fits indicated

343   the photogrammetric approach performed as well as widely used *in situ* allometric

344   approaches at the species-level (Fig. 1, Table 1, Supplementary Fig. 1, Supplementary

345   Table 2)[15,22,41,42]. Importantly, however, intensive drone surveys are relatively easy to

346   conduct over larger spatial extents of several hectares. Using a carefully designed,

347   standardised protocol[33] for acquiring and processing datasets yielded a good level of

348   success in reconstructing 93% (688/741) of plots (Fig. 1C). The few instances where

349   reconstructions were unsuccessful include mosses in rocky terrain, tall and dense grassland,

350   and taller trees and shrubs (> 3 m) and are discussed in Supplementary Note 1. The

351   similarities of the height-biomass relationships indicate this approach is generalisable across

352   growth forms and environmental settings.

353

354   At the PFT-level, we found canopy height strongly predicted AGB across all six PFTs, with

355   adjusted R^2 ranging from 0.49 to 0.99 (Fig. 2, Table 1). For every 1-centimetre increase in

356   mean canopy height, AGB increased by between 11 to 115 g m^{-2}, depending on PFT (Fig. 2,

357   Table 1). Ferns had the lowest density (1,096 g m^{-3}), followed by forbs (1,191 g m^{-3}), then

358   graminoids (2,898 g m^{-3}) and shrubs (3,214 g m^{-3}) with notably similar densities, then small

359   trees (5,572 g m^{-3}) and lastly succulents had the largest density (11,532 g m^{-3}). Species-level

360   model slopes were generally similar *within,* but different *between,* PFTs. The similarity of

361   densities within PFTs indicates these relationships are generally transferrable between

362   species within PFTs, particularly for the better sampled types such as graminoids and

363   shrubs, although phenotypic and phenological variation will limit accuracy[31,41]. Should

364   destructive harvests for local calibrations not be possible due to resource limitations or taxon

365 conservation status, the height-mass models described here could be used to non-

366 destructively estimate AGB from similar drone-derived canopy height models (Table 1 and

367 Supplementary Table 2). These allometric relationships were linear across the range of

368 canopy height and biomass that we sampled, allowing their application from the whole plant-

369 level to the ecosystem-level without necessarily requiring the discrete analysis of individual

370 plants that can be challenging in ecosystems with coalesced canopies[14,27,31,43].

371
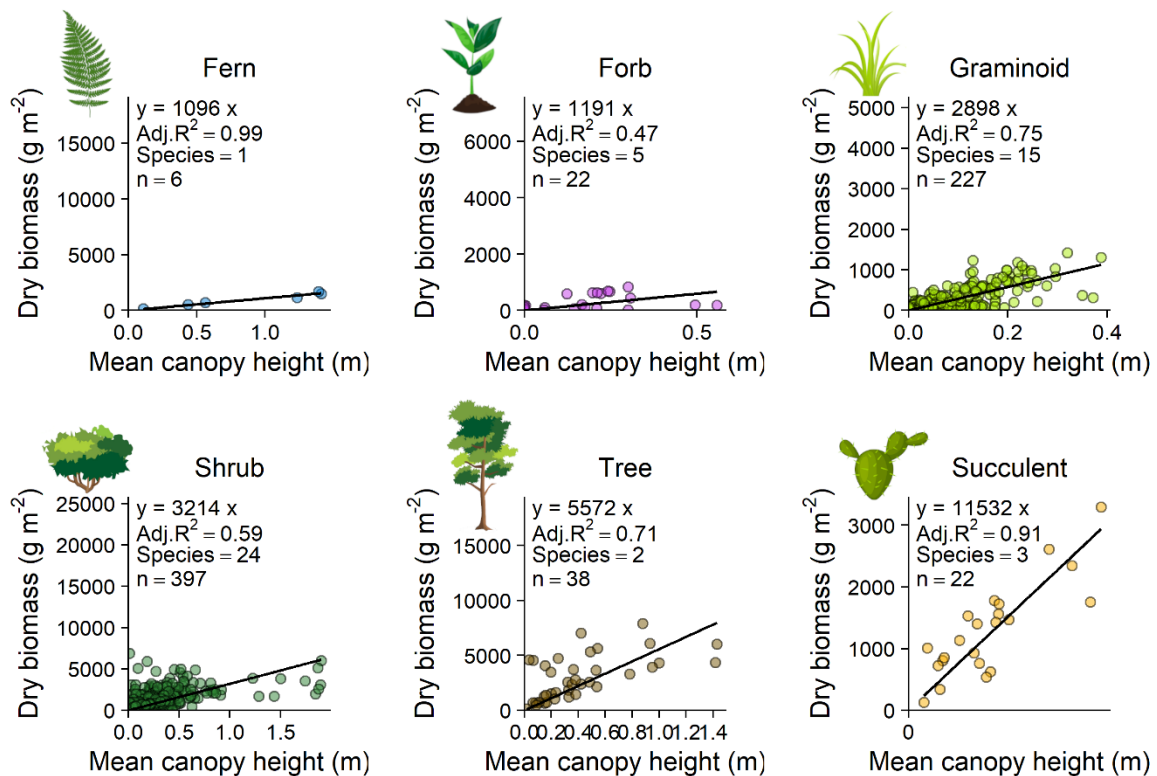
372

373 **Fig. 2. Photogrammetrically derived canopy height was a strong predictor of biomass**

374 **within plant functional types.** A constant X:Y ratio was used for all plots, so model slopes

375 can be compared visually even though axis ranges vary. Model slopes were generally similar

376 within, but differed between, plant functional types. 'Species' indicates the number of species

377 pooled for each plant functional type and black lines are linear models with intercepts

378 constrained through the origin. Full model results are included in Table 1.

379   Table 1. Parameters for linear models fitted to each plant functional type. LOOCV is the

380   prediction error from Leave-One-Out Cross-Validation divided by the slope.

Plant functional type	n	n of surveys	Slope	Residual standard error	Adj. R^2	t-statistic	P value	LOOCV
			g m^{-2}	g m^{-2}				%
Fern	6	1	1,096	53	0.99	20.558	<0.0001	12.0
Forb	22	3	1,191	262	0.47	4.534	0.0002	19.0
Graminoid	227	17	2,898	112	0.75	25.786	<0.0001	3.7
Shrub	397	24	3,214	134	0.59	23.823	<0.0001	11.6
Succulent	22	3	11,532	760	0.91	15.159	<0.0001	2.6
Tree	38	2	5,572	577	0.71	9.654	<0.0001	16.7

381

382   Wind speed negatively affected canopy heights reconstructed from photogrammetry (Fig.

383   3A, Supplementary Table 3, Supplementary Fig. 2, Supplementary Fig. 3, Supplementary

384   Note 2). We found the height-wind interaction parameter was strongly positive and highly

385   significant ($p < 0.0001$) (Fig. 3A Supplementary, Table 3). This influence was seen at both

386   the PFT-level (Supplementary Fig. 2A) and species-level (Supplementary Fig. 3). Biomass

387   divided by height increased for surveys conducted in windier conditions, because the

388   movement of foliage meant lower mean canopy heights were reconstructed from images that

389   were acquired non-concurrently (see Supplementary Note 2 for extended discussion).

390   However, wind effects had only limited influence in our study because most of our plots were

391   surveyed in relatively light wind conditions (of < 4 m s^{-1}) (Supplementary Fig. 2A). We expect

392   sensitivity to wind speed differs between species because the effects of wind on foliage

393   motion depend on canopy architecture and mechanical properties like limb stiffness[44]

394   (Supplementary Fig. 3, Supplementary Note 2). Previous studies in forest settings have

395   reported contradictory effects of wind speed on canopy reconstructions[30,35], but we think that

396   these differences are linked with the spatial grain of analysis. Our study demonstrates the

397   need to control for the influence of wind speed in future work particularly when surveying

398   low-stature plant canopies.

399

400   Sun elevation had no effect on allometric density and by extension reconstructed plant

401   height (Fig. 3B, Supplementary Fig. 2B, Supplementary Fig. 5, Supplementary Table 5).

402   Cloudy conditions appeared to have a notable effect on allometric density; however, the

403   imbalance in observations under cloudy and clear conditions (n=80 and n=620,

404   respectively), meant this effect was not considered reliable (Supplementary Table 4,

405   Supplementary Fig. 4). As with wind, previous studies in forest settings reported

406   contradictory effects of elevation on canopy reconstructions[30,35]. However, illumination

407   conditions affect photogrammetry in complex ways[37,45], with the influence of sun elevation

408   depending on the distribution and intensity of shadows as well as the properties of the

409   camera sensor and user choices during processing (see Supplementary Note 3 for extended

410   discussion). When comparing findings regarding illumination effects, it is therefore necessary

411   to consider the capabilities of the sensors and workflows employed and the structural

412   complexities of the observed ecosystems. Our findings suggest that surveying under low

413   wind speeds may be a higher priority than optimal illumination conditions for obtaining

414   structural models of vegetation in low stature ecosystems.

415

416
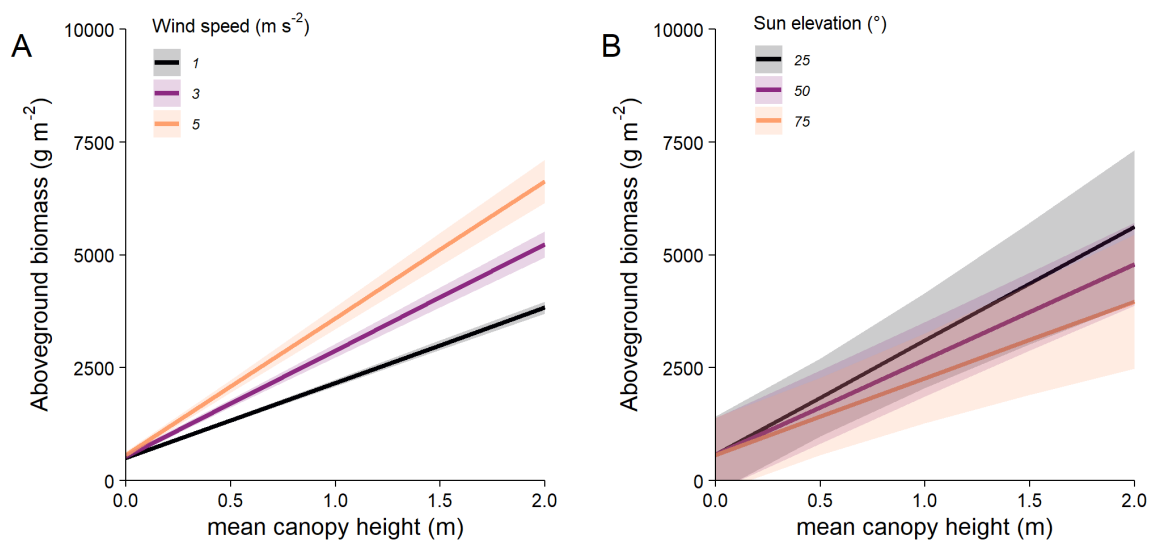
Fig. 3. Reconstructed plant height and thus height-biomass relationships were systematically influenced by wind speed but were insensitive to illumination conditions. Mean predicted aboveground biomass variation over the range of observed mean canopy height, estimated for a range of three wind speeds and sun elevations. Wind speed has a statistically clear and positive effect on the relationship between height and biomass (**A**) (Supplementary Figs. 2A and 3, Supplementary Table 3), but sun elevation had no significant effect on the relationship between height and biomass (**B**) (Supplementary Figs. 2B and 5, Supplementary Table 5). Shaded areas represent 95% confidence intervals on the model predictions.

426   **Discussion**

427   We established accurate height-biomass relationships for non-forest vegetation using

428   standardised drone photogrammetry protocols. Our findings enable observations that will

429   provide new insights into ecosystem dynamics at previously understudied scales across

430   non-forested ecosystems. Linear models have strong correspondence with observations at

431   the species and PFT-levels across a diverse range of low-stature ecosystems and perform

432   as well as conventional *in situ* allometric approaches reported in the literature (Table 1, Fig.

433   2, Supplementary Table 2 and Supplementary Fig. 1). The similarity of graminoid and shrub

434   PFT relationships indicate these could be applied together to estimate AGB in mixed

435   ecosystems, without the need to individually classify these taxa, although there will be cases

436   where allometric functions will need to be calibrated locally (Supplementary Note 4). As

437   mean canopy height is readily compared between taxa, ecosystems and observation

438   approaches[14,22], these linear allometric relationships are straightforward to interpret[46] and

439   can be easily integrated with landscape modelling frameworks. Drone photogrammetry is a

440   relatively 'low-cost' (although see Supplementary Note 5) tool well suited for local-scale

441   observation in non-forest ecosystems. The ease of surveying landscape scales of 1 to 10 ha

442   is critical to advancing beyond existing *in situ* approaches and overcoming the gap between

443   on-the-ground monitoring and the coarser grain of global-scale products derived from

444   satellite-based remote sensing[27,31]. Accurate information at these intermediary scales is

445   invaluable for validating models and testing the scaling of ecological relationships and

446   biomass carbon estimates from plots to biomes[6].

447

448   Addressing critical knowledge gaps in plant science with drone photogrammetry requires

449   standardised protocols, such as those used here, because photogrammetry-derived models

450   are sensitive to the ways in which data are collected[27,30,35–38], processed[27,36–38], and

451   analysed[20,27–29]. These sensitivities can be more pronounced for subjects with complex

452   texture, such as vegetation, and hinder comparisons between products obtained from

453   different workflows. To date, what has been missing are systematic and reproducible

454   demonstrations of how drone data can be used in real-world plant ecology research. Using

455   standardised protocols, we established comparable height-biomass relationships for a wide

456   range of low-stature plant species for the first time and enable investigation of how factors

457   such as wind speed (Fig. 3A), illumination (Fig. 3B)[35], or antecedent conditions[41] may

458   influence allometric approaches. We show that it is important to account for the effects of

459   wind speed during photogrammetric surveys beyond simply considering the effects of wind

460   on drone platforms. The most reproducible reconstructions will be obtained under 'zero' wind

461   speeds[30,35,37], but this is often not possible under real world operational conditions[31,45,47]. Our

462   findings demonstrate that data will be most comparable when wind speeds are similar, but

463   also that, where differences are unavoidable, it will be possible to derive corrections for how

464   wind influences canopy reconstructions from drone photogrammetry. We call for the

465   continued development of harmonised and community-based protocols to maximise

466   knowledge gains and support cross-biome syntheses[31,33,34,48].

467

468   Our findings show drone photogrammetry can yield informative canopy height models

469   capable of detecting ecologically significant differences in AGB across a diverse range of

470   low-stature ecosystems globally. Drones have considerable advantages as data collection

471   platforms for ecological applications, including their relatively low cost, versatility in

472   deployment allowing high temporal resolution monitoring, and capacity to record fine-grained

473   and spatially explicit data[34,45,49]. Systematic and comparable observations of plant canopy

474   structure and biomass are vital for calibrating and evaluating vegetation models and biomass

475   products retrieved from globally-available remote sensing systems[1,32,50,51]. Drone data

476   collection can broaden the scope of research and monitoring programmes to obtain more

477   representative observations in vulnerable and understudied low-stature ecosystems.

478   Photogrammetric approaches for monitoring canopy height and biomass provide novel tools

479   that should be used more widely by the ecological research community to improve

480   assessments of ecosystem change and global carbon budgets.

481

482

483   **Data availability**

484   Data collected for this publication, including aerial images, marker and plot coordinates, and

485   dry sample weights, as well as site and survey metadata, are available from the NERC

486   Environmental Information Data Centre (DOI: <DATA DEPOSIT IN PROGRESS> -

487   AVAILABLE ON REQUEST IF REQUIRED FOR REVIEW). Code for photogrammetric

488   processing and statistical analysis is available at <https://github.com/AndrewCunliffe/Global-

489   Drone-Allometry>.

References

490   **References**

491   1.   Duncanson, L. *et al.* The importance of consistent global forest aboveground biomass

492   product validation. *Surv Geophys* **40**, 979–999 (2019).

493   2.   Liu, Y. Y. *et al.* Recent reversal in loss of global terrestrial biomass. *Nature Climate*

494   *Change* **5**, 470–474 (2015).

495   3.   Ahlström, A. *et al.* The dominant role of semi-arid ecosystems in the trend and variability

496   of the land CO2 sink. *Science* **348**, 895–899 (2015).

497   4.   Poulter, B. *et al.* Contribution of semi-arid ecosystems to interannual variability of the

498   global carbon cycle. *Nature* **509**, 600–603 (2014).

499   5.   Asner, G. P., Elmore, A. J., Olander, L. P., Martin, R. E. & Harris, A. T. Grazing Systems,

500   Ecosystem Responses, and Global Change. *Annual Review of Environment and*

501   *Resources* **29**, 261–299 (2004).

502   6.   Myers-Smith, I. H. *et al.* Complexity revealed in the greening of the Arctic. *Nat. Clim.*

503   *Chang.* **10**, 106–117 (2020).

504   7.   McNicol, I. M., Ryan, C. M. & Mitchard, E. T. A. Carbon losses from deforestation and

505   widespread degradation offset by extensive growth in African woodlands. *Nature*

506   *Communications* **9**, 3045 (2018).

507   8.   Sleeter, B. M. *et al.* Effects of contemporary land-use and land-cover change on the

508   carbon balance of terrestrial ecosystems in the United States. *Environ. Res. Lett.* **13**,

509   045006 (2018).

510   9.   Meilhac, J., Deschamps, L., Maire, V., Flajoulot, S. & Litrico, I. Both selection and

511   plasticity drive niche differentiation in experimental grasslands. *Nat. Plants* **6**, 28–33

512   (2020).

513   10. Meilhac, J., Durand, J.-L., Beguier, V. & Litrico, I. Increasing the benefits of species

514   diversity in multispecies temporary grasslands by increasing within-species diversity.

515   *Ann Bot* **123**, 891–900 (2019).

516   11. Myers-Smith, I. H. *et al.* Eighteen years of ecological monitoring reveals multiple lines of

517   evidence for tundra vegetation change. *Ecol. Monogr.* **89**, (2019).

518   12. Harper, A. B. *et al.* Land-use emissions play a critical role in land-based mitigation for

519   Paris climate targets. *Nat Commun* **9**, 1–13 (2018).

520   13. Griscom, B. W. *et al.* Natural climate solutions. *PNAS* **114**, 11645–11650 (2017).

521   14. Bartsch, A. *et al.* Feasibility of tundra vegetation height retrieval from Sentinel-1 and

522   Sentinel-2 data. *Remote Sensing of Environment* **237**, 111515 (2020).

523   15. Huenneke, L. F., Clason, D. & Muldavin, E. Spatial heterogeneity in Chihuahuan Desert

524   vegetation: implications for sampling methods in semi-arid ecosystems. *Journal of Arid*

525   *Environments* **47**, 257–270 (2001).

526   16. Shriver, R. K. Quantifying how short-term environmental variation leads to long-term

527   demographic responses to climate change. *Journal of Ecology* **104**, 65–78 (2016).

528   17. Schimel, D. *et al.* Observing terrestrial ecosystems and the carbon cycle from space.

529   *Glob Change Biol* **21**, 1762–1776 (2015).

530   18. Bendig, J. *et al.* Estimating Biomass of Barley Using Crop Surface Models (CSMs)

531   Derived from UAV-Based RGB Imaging. *Remote Sensing* **6**, 10395–10412 (2014).

532   19. Kröhnert, M. *et al.* Watching grass grow - a pilot study on the suitability of

533   photogrammetric techniques for quantifying change in aboveground biomass in

534   grassland experiments. in *ISPRS - International Archives of the Photogrammetry,*

535   *Remote Sensing and Spatial Information Sciences* vol. XLII–2 539–542 (Copernicus

536   GmbH, 2018).

537   20. Grüner, E., Astor, T. & Wachendorf, M. Biomass prediction of heterogeneous temperate

538   grasslands using an SfM approach based on UAV imaging. *Agronomy* **9**, 54 (2019).

539   21. Wijesingha, J., Moeckel, T., Hensgen, F. & Wachendorf, M. Evaluation of 3D point cloud-

540   based models for the prediction of grassland biomass. *International Journal of Applied*

541   *Earth Observation and Geoinformation* **78**, 352–359 (2019).

542   22. Cunliffe, A. M., Assmann, J., Daskalova, G., Kerby, J. T. & Myers-Smith, I. H.

543   Aboveground biomass corresponds strongly with drone-derived canopy height but

544   weakly with greenness (NDVI) in a shrub tundra landscape. *Environmental Research*

545   *Letters* (2020) doi:10.1088/1748-9326/aba470.

546   23. Greaves, H. E. Applying Lidar and High-Resolution Multispectral Imagery for Improved

547   Quantification and Mapping of Tundra Vegetation Structure and Distribution in the

548   Alaskan Arctic. (University of Idaho, 2017).

549   24. Dubayah, R. *et al.* The Global Ecosystem Dynamics Investigation: high-resolution laser

550   ranging of the Earth's forests and topography. *Science of Remote Sensing* 100002

551   (2020) doi:10.1016/j.srs.2020.100002.

552   25. Westoby, M. J., Brasington, J., Glasser, N. F., Hambrey, M. J. & Reynolds, J. M.

553   'structure-from-motion' photogrammetry: A low-cost, effective tool for geoscience

554   applications. *Geomorphology* **179**, 300–314 (2012).

555   26. Dandois, J. P. & Ellis, E. C. High spatial resolution three-dimensional mapping of

556   vegetation spectral dynamics using computer vision. *Remote Sensing of Environment*

557   **136**, 259–276 (2013).

558   27. Cunliffe, A. M., Brazier, R. E. & Anderson, K. Ultra-fine grain landscape-scale

559   quantification of dryland vegetation structure with drone-acquired structure-from-motion

560   photogrammetry. *Remote Sens. Environ.* **183**, 129–143 (2016).

561   28. Wallace, L., Hillman, S., Reinke, K. & Hally, B. Non-destructive estimation of above-

562   ground surface and near-surface biomass using 3D terrestrial remote sensing

563   techniques. *Methods in Ecology and Evolution* **8**, 1607–1616 (2017).

564   29. Lussem, U. *et al.* Estimating biomass in temperate grassland with high resolution canopy

565   surface models from UAV-based RGB images and vegetation indices. *JARS* **13**, 034525

566   (2019).

567   30. Frey, J. *et al.* UAV Photogrammetry of Forests as a Vulnerable Process. A Sensitivity

568   Analysis for a Structure from Motion RGB-Image Pipeline. *Remote Sensing* **10**, 912

569   (2018).

570   31. Poley, L. & McDermid, G. A systematic review of the factors influencing the estimation of

571   vegetation aboveground biomass using unmanned aerial systems. *Remote Sensing* **12**,

572   1052 (2020).

573   32. Bouvet, A. *et al.* An above-ground biomass map of African savannahs and woodlands at

574   25m resolution derived from ALOS PALSAR. *Remote Sensing of Environment* **206**, 156–

575   173 (2018).

576   33. Cunliffe, A. & Anderson, K. Measuring Above-ground Biomass with Drone

577   Photogrammetry: Data Collection Protocol. *Protocol Exchange* (2019)

578   doi:10.1038/protex.2018.134.

579   34. Tmušić, G. *et al.* Current Practices in UAS-based Environmental Monitoring. *Remote*

580   *Sensing* **12**, 1001 (2020).

581   35. Dandois, J. P., Olano, M. & Ellis, E. C. Optimal altitude, overlap, and weather conditions

582   for computer vision UAV estimates of forest structure. *Remote Sensing* **7**, 13895–13920

583   (2015).

584   36. James, M. R. & Robson, S. Mitigating systematic error in topographic models derived

585   from UAV and ground-based image networks. *Earth Surf. Process. Landforms* **39**, 1413–

586   1420 (2014).

587   37. Mosbrucker, A. R., Major, J. J., Spicer, K. R. & Pitlick, J. Camera system considerations

588   for geomorphic applications of SfM photogrammetry. *Earth Surface Processes and*

589   *Landforms* **42**, 969–986 (2017).

590   38. James, M. R., Antoniazza, G., Robson, S. & Lane, S. N. Mitigating systematic error in

591   topographic models for geomorphic change detection: Accuracy, precision and

592   considerations beyond off-nadir imagery. *Earth Surface Processes and Landforms*

593   (2020) doi:10.1002/esp.4878.

594   39. Pätzig, M., Geiger, F., Rasche, D., Rauneker, P. & Eltner, A. Allometric relationships for

595   selected macrophytes of kettle holes in northeast Germany as a basis for efficient

596   biomass estimation using unmanned aerial systems (UAS). *Aquatic Botany* **162**, 103202

597   (2020).

598   40. Whittaker, R. H. *Communities and Ecosystems*. (MacMillan Publishing Co, 1975).

599   41. Rudgers, J. A. *et al.* Sensitivity of dryland plant allometry to climate. *Functional Ecology*

600   **32**, 2290–2303 (2019).

601   42. Muldavin, E. H., Moore, D. I., Collins, S. L., Wetherill, K. R. & Lightfoot, D. C.

602   Aboveground net primary production dynamics in a northern Chihuahuan Desert

603   ecosystem. *Oecologia* **155**, 123–132 (2008).

604   43. Krofcheck, D., Litvak, M., Lippitt, C. & Neuenschwander, A. Woody Biomass Estimation

605   in a Southwestern U.S. Juniper Savanna Using LiDAR-Derived Clumped Tree

606   Segmentation and Existing Allometries. *Remote Sensing* **8**, 453 (2016).

607   44. Rowe, N. & Speck, T. Plant growth forms: an ecological and evolutionary perspective.

608   *New Phytologist* **166**, 61–72 (2005).

609   45. Aber, J. S., Marzolff, I, Ries, J. & Aber, S. W. *Small Format Aerial Photography and UAS*

610   *imagery: Principles, techniques and geoscience applications*. (Elsevier, 2019).

611   46. Warton, D. I., Wright, I. J., Falster, D. S. & Westoby, M. Bivariate linefitting methods for

612   allometry. *Biological Reviews* 259–291 (2006).

613   47. Duffy, J. P. *et al.* Location, location, location: considerations when using lightweight

614   drones in challenging environments. *Remote. Sens. Ecol. Conserv.* **4**, 7–19 (2017).

615   48. Pérez-Harguindeguy, N. *et al.* New handbook for standardised measurement of plant

616   functional traits worldwide. *Aust. J. Bot.* **61**, 167–234 (2013).

617   49. Anderson, K. & Gaston, K. J. Lightweight unmanned aerial vehicles (UAVs) will

618   revolutionise spatial ecology. *Frontiers in Ecology and Environment* **11**, 138–146 (2013).

619   50. Tian, F. *et al.* Remote sensing of vegetation dynamics in drylands: Evaluating vegetation

620   optical depth (VOD) using AVHRR NDVI and in situ green biomass data over West

621   African Sahel. *Remote Sensing of Environment* **177**, 265–276 (2016).

622   51. Rodríguez-Fernández, N. J. *et al.* An evaluation of SMOS L-band vegetation optical

623   depth (L-VOD) data sets: high sensitivity of L-VOD to above-ground biomass in Africa.

624   *Biogeosciences* **15**, 4627–4645 (2018).

625 52. Herold, M. *et al.* The role and need for space-based forest biomass-related

626   measurements in environmental management and policy. *Surv Geophys* **40**, 757–778

627   (2019).

628 53. Luhmann, T., Fraser, C. & Maas, H.-G. Sensor modelling and camera calibration for

629   close-range photogrammetry. *ISPRS Journal of Photogrammetry and Remote Sensing*

630   **115**, 37–46 (2016).

631 54. James, M. R., Robson, S., d'Oleire-Oltmanns, S. & Niethammer, U. Optimising UAV

632   topographic surveys processed with structure-from-motion: Ground control quality,

633   quantity and bundle adjustment. *Geomorphology* **280**, 51–66 (2017).

634 55. Hendrickx, H. *et al.* The reproducibility of SfM algorithms to produce detailed Digital

635   Surface Models: the example of PhotoScan applied to a high-alpine rock glacier.

636   *Remote Sensing Letters* **10**, 11–20 (2019).

637 56. Nesbit, P. R. & Hugenholtz, C. H. Enhancing UAV-SfM 3D model accuracy in high-relief

638   landscapes by incorporating oblique images. *Remote Sensing* **11**, undefined-undefined

639   (2019).

640 57. Chudley, T. R., Christoffersen, P., Doyle, S. H., Abellan, A. & Snooke, N. High-accuracy

641   UAV photogrammetry of ice sheet dynamics with no ground control. *The Cryosphere* **13**,

642   955–968 (2019).

643 58. Zhang, H. *et al.* Evaluating the potential of post-processing kinematic (PPK)

644   georeferencing for UAV-based structure- from-motion (SfM) photogrammetry and

645   surface change detection. *Earth Surface Dynamics* **7**, 807–827 (2019).

646 59. Cunliffe, A. M. *et al.* Allometric relationships for predicting aboveground biomass and

647   sapwood area of Oneseed Juniper (Juniperus monosperma) trees. *Front. Plant Sci.* **11**,

648   (2020).

649 60. Ribeiro-Gomes, K., Hernandez-Lopez, D., Ballesteros, R. & Moreno, M. A. Approximate

650   georeferencing and automatic blurred image detection to reduce the costs of UAV use in

651   environmental and agricultural applications. *Biosystems Engineering* **151**, 308–327

652   (2016).

653   61. Wilke, N. *et al.* Quantifying lodging percentage and lodging severity using a UAV-based

654   canopy height model combined with an objective threshold approach. *Remote Sensing*

655   **11**, 515 (2019).

656   62. PDAL Contributors. *PDAL Point Data Abstraction Library*. (2020).

657   63. R Core Team. *R: A language and environment for statistical computing.* (R Foundation

658   for Statistical Computing, 2019).

659   64. Kennedy, S. *Astral.* (2020).

660   65. Stefan, V. *plotbiomes: Plot Whittaker biomes with ggplot2*. (2018).

661   66. Alfons, A. *cvTools*. (2015).

662   67. Bates, D., Mächler, M., Bolker, B. & Walker, S. Fitting Linear Mixed-Effects Models

663   Using {lme4}. *Journal of Statistical Software* **67**, 1–48 (2015).

664   68. Lüdecke, D. & Aust, F. *ggeffects*. (2020).

665   69. Krzywinski, M. & Altman, N. Error bars. *Nature Methods* **10**, 921–922 (2013).

666   70. Kuznetsova, A., Brockhoff, P. B., Christensen, R. & Jensen, S. *lmerTest*. (2020).

667   71. Assmann, J. J., Kerby, J. T., Cunliffe, A. M. & Myers-Smith, I. H. Vegetation monitoring

668   using multispectral sensors - best practices and lessons learned from high latitudes.

669   *Journal of Unmanned Vehicle Systems* 334730 (2018) doi:10.1101/334730.

670   72. Lüdecke, D., Makowski, D., Waggoner, P. & Patil, I. *performance*. (2020).

671

Acknowledgements

ORCIDs

A.M.C.: 0000-0002-8346-4278, K.A.: 0000-0002-3289-2598, F.B.: 0000-0002-7612-3264, H.A.G.: 0000-0001-9451-5010, R.E.B.: 0000-0002-8715-0399, I.H.M.-S.: 0000-0002-8417-6112, T.A.: 0000-0003-4608-955X, M.M.B.: 0000-0001-6362-4572, L.C.: 0000-0003-3710-0817, P.E.C.: 0000-0003-4299-1853, M.D.C.: 0000-0003-0989-3266, M.S.E.-L.: 0000-0002-0541-3053, S.M.E.: 0000-0002-7246-2795, J.M.F.-G.: 0000-0002-6065-3981, A.G.F.: 0000-0002-6903-8053, K.G.: 0000-0002-6943-9172, B.M.G.: 0000-0003-1464-3747, A.G.: 0000-0002-4476-8279, N.P.H.: 0000-0002-9130-5306, M.S.H.: 0000-0001-7275-9145, S.H.: 0000-0002-5702-4236, C.A.H.: 0000-0003-3913-0980, P.H.: 0000-0002-1073-4564, W.J.: 0000-0003-2554-4373, J.W.K.: 0000-0002-3326-3806, M.K.: 0000-0001-8773-8005, S.K.: 0000-0001-8849-8162, M.B.L.: 0000-0003-3960-3522, I.M.: 0000-0002-0917-4336, M.E.M: 0000-0001-8733-9119, C.D.M.: 0000-0001-9666-5805, D.M.: 0000-0002-0330-8698, L.A.M.-B.: 0000-0001-7467-5498, S.C.P.: 0000-0001-6310-0146, J.P.: 0000-0001-9982-2730, E.S.-A.: 0000-0001-9975-5726, K.J.S.: 0000-0002-2153-8534, D.S.-B.: 0000-0001-8215-975X, P.S.: 0000-0003-2480-1171, S.S.: 0000-0003-1821-8561, J.S.: 0000-0001-8664-8059, C.S.: 0000-0003-3480-3023, S.S.-S.: 0000-0001-7656-4214, S.A.V.: 0000-0002-0052-8580, M.L.V.: 0000-0003-0720-1422, F.V.: 0000-0001-6042-9341, M.W.: 0000-0002-2840-7086, H.W.: 0000-0003-1777-5067, R.W.: 0000-0001-8496-3514

Author contributions

727

728 A.M.C. conceived the research idea, administered the project, curated the data, did the data
729 visualisation and led the writing of the manuscript. A.M.C. and K.A. developed the
730 experimental design. A.M.C., K.A., R.E.B., I.H.M.-S., M.M.B., P.E.C., M.D.C., J.M.F.-G.,
731 A.G., N.P.H., C.A.H., P.H., J.W.K., I.M., L.A.M.-B., S.C.P., J.P., S.S., J.S., S.A.V. and M.L.V.
732 acquired funding. A.M.C., K.A., F.B., R.E.B., I.H.M.-S., T.A., M.M.B., L.C., P.E.C., M.D.C.,
733 M.S.E.-L., S.M.E., J.M.F.-G., A.G.F., K.G., B.M.G., A.G., N.P.H., M.S.H., S.H., C.A.H., P.H.,
734 W.J., J.W.K., M.K., S.K., M.B.L., I.M., M.E.M, C.D.M., D.M., L.A.M.-B., S.C.P., J.P., E.S.-A.,
735 K.J.S., D.S.-B., P.S., S.S., J.S., C.S., S.S.-S., S.A.V., M.L.V., F.V., M.W., H.W. and R.W.
736 undertook the investigation. A.M.C. and H.A.G. developed the processing program. A.M.C.,
737 I.H.M.-S. and H.A.G. performed the analysis. All authors contributed to the final version of
738 the manuscript.

739

Competing interests

740

741 The authors declare no competing financial interests.